Bulgarian Academy of Sciences
Institute of Chemical Engineering

Eng. Stela Plamenova Panyovska

CFD MODELING OF MEMBRANE SEPARATION THROUGH NANOFILTRATION

S U M M A R Y

Scientific consultants: Prof. PhD. Daniela Dzhonova – Atanasova
Prof. PhD. Iren Tsibranska

Sofia, 2025

Bulgarian Academy of Sciences

Institute of Chemical Engineering

Eng. Stela Plamenova Panyovska

CFD MODELING OF MEMBRANE SEPARATION THROUGH NANOFILTRATION

S U M M A R Y

of a dissertation for an educational and scientific degree "PhD"

Field of higher education: 4. Natural sciences, mathematics and informatics

Professional field: 4.2. Chemical Sciences

PhD program: Processes and apparatus in chemical and biochemical technology

Scientific consultants: Prof. PhD. Daniela Dzhonova – Atanasova

Prof. PhD. Iren Tsibranska

Scientific jury:

1. Prof. PhD Tatyana Stefanova Petrova
2. Assoc. Prof. PhD Petya Georgieva Popova-Krumova
3. Assoc. Prof. PhD Stella Ivanova Minkovska
4. Prof. PhD Iliya Krastev Iliev
5. Prof. PhD Nina Yankova Penkova

The dissertation contains: 151 pages, 62 figures and 2 tables. The bibliography includes 169 literary sources.

The Numerical modeling was carried out at the Institute of Chemical Engineering - Bulgarian Academy of Sciences

The dissertation defense will take place at:
..... from ..... hours
at the Institute of Chemical Engineering - BAS, Sofia, “Acad. Georgi Bonchev” Str., block 103

Topic: CFD MODELING OF MEMBRANE SEPARATION THROUGH NANOFILTRATION

Author: Eng. Stela Plamenova Panyovska

Materials are available in the office of the Institute of Chemical Engineering - BAS.

Contents

SYMBOLS USED		
MEANING	**PHYSICAL MEANING**	**SI**
ρ	Density	$\kappa g/m^3$
t	Time	s
d	Diameter	m
h	Height	m
d_e	Sensor diameter	m
d_h	Hydraulic diameter	m
v_f	feed inlet velocity	m/s
k_L	Local mass transfer coefficient	m/s
k_m	Average mass transfer coefficient	m/s
A	Area	m^2
V	Volume	L
J	Permeate flux	L/m^2h
N	Stirrer speed	rpm
μ	Dynamic viscosity	Pa.s
τ	Wall shear stress	Pa
ν	Kinematic viscosity	m2/s
D	Diffusion coefficient	m^2s
k_m	Local value of mass transfer coefficient	m/s
k_{max}	Maximum value of mass transfer	m/s
E_{ff}	Efficiency coefficient	
D_{cell}	Cell diameter	m
$d_{in/out}$	Inlet and outlet diameter	m
Q_f	Flow rate	l/min
v_f	Flow velocity	m/s
CFR	Cross-flow rate	L/h

ABCRONYMS USED		
NF	Nanofiltration	
RO	Reverse Osmosis	
UF	Ultrafiltration	
MBR	Membrane Bioreactor	
CFD	Computational Fluid Dynamics	
DE	Dead-End Filtration	
CF	Cross-Flow Filtration	
Sh	Sherwood number	
Re	Reynolds number	
Sc	Schmidt number	
RANS	Reynolds-averaged Navier–Stokes equation	
k-ε	Realizable k-ε model	
MRF	Moving reference frame	
CFR	Cross-flow rate	

I. Introduction

Nanofiltration (NF) is a membrane process that bridges the gap between reverse osmosis (RO) and ultrafiltration (UF) in terms of particle size, selectivity, and operating pressure. Introduced in the late 1980s, nanofiltration has seen rapid growth in its applications. NF technology continues to develop, finding new uses in drinking water production, wastewater treatment, and the food, chemical, and pharmaceutical industries, among many others. Despite its promising prospects, several unresolved issues still hinder large-scale implementation. Membrane fouling—which reduces membrane flux, lifespan, and overall efficiency—remains a significant challenge for the scientific community.

Membrane Bioreactor (MBR) technologies provide biological treatment through membrane separation. Today, MBRs have numerous domestic and industrial applications and are widely used compared to conventional methods. The main disadvantage of MBR operation is membrane fouling, which leads to a decrease in permeate flux and necessitates membrane cleaning. Although significant progress has been made in recent decades toward developing improved techniques to reduce fouling, a variety of physical and mechanical methods are still required to further mitigate membrane fouling problems. Various studies have been conducted to enhance the applicability of nanofiltration. Research has shown that Computational Fluid Dynamics (CFD) is a valuable tool for providing a comprehensive analysis of the membrane filtration process. CFD is effectively used to model membrane separation processes and supports the design and optimization of membrane bioreactors and membrane modules. Specifically, CFD modeling aids in the design and optimization of submerged (MBRs) by analyzing fluid flow, separation dynamics of submerged membranes, mass transfer rates, and fouling conditions. [1, 14]. Models of increased complexity are

also being developed, taking into account the relationship between reaction kinetics in the bioreactor and the filtration process together with the hydrodynamic conditions in an integrated MBR [1]. The solute distribution within the concentration polarization layer and the effect of the increased concentration at the membrane interface has been solved: both for steady and unsteady-state conditions [2]; in dead-end (stirred and unstirred) [3]; and cross-flow filtration mode [2, 4]. alone or in combination with the membrane layer [5], or the gel layer growth at the membrane surface [6].

Hydrodynamic models primarily focus on fouling, as the reduction and/or control of fouling can be achieved through process hydrodynamics, particularly by creating favorable conditions near the membrane surface. By inducing shear stress, promoting fluid turbulence, and enhancing the convective transport of particles away from the membrane, significant reductions in fouling can be obtained. Special attention is given to membrane fouling - including multidimensional fouling [1] in MBRs with different membrane geometries (flat sheet, tubular, hollow fiber) [4, 5, 7, 8, 9] as well as to the effects of gas bubbles [10, 11, 12] stirring [1] and the introduction of additional energy (vibrations, membrane movement) [13].

CFD is widely applied in such investigations [14], with a focus on understanding shear-stress distribution along the membrane surface. Shear stress is primarily influenced by stirring (the flow pattern generated by the impeller), fluid viscosity (particularly in fluids with complex rheology), and gas bubbling in aerated MBRs (bubble size and gas flow rate).

The application of CFD to describe mass transfer through membranes involves various approaches to representing the membrane within the model and still poses a challenge for researchers. Published studies demonstrate the potential of CFD modeling primarily for predicting hydrodynamic conditions in membrane reactors or membrane modules of a

given geometry, and to a lesser extent for investigating mass transfer through the membrane.

The working hypothesis in studying mass transfer is that sufficient model accuracy can be achieved. This would allow the simulation of conditions in the concentration polarization layer and provide reliable estimates of the mass transfer coefficients in the region near the membrane.

To evaluate the efficiency of the integrated process, a detailed investigation of the flow behavior in the MBR and the transport of individual components is necessary. Both issues ultimately come down to assessing the mass transfer rate across the membrane surface. Numerous studies and publications address mass transfer; however, the parameter used to represent MBR mass transfer efficiency—which serves to compare different MBR configurations—is rarely mentioned or emphasized. Assuming the effectiveness E_{ff} is defined as the degree of achievement of a target value, it should be expressed in relative terms, that is, as a ratio of k_m values. A proper approach is to take the ratio of the local k_m value, corresponding to the local velocity gradient, to an extreme value k_{max}, which represents the maximum desirable target value attainable under the most favorable operating conditions.

$$E_{ff} = \frac{k_m}{k_{max}} \tag{1}$$

In this way, an E_{ff} value can be assigned to the different zones of the membrane module. Moreover, if based on a widely accepted standard, it would be possible to compare the effectiveness E_{ff} of different membrane units.

II . Aim and Objectives

1. Aim

The main aim of the dissertation is mathematical modeling of hydrodynamics and mass transfer in nanofiltration in order to determine optimal process conditions in the following configurations:

1) Dead-End filtration cell with agitator and flat bottom membrane;

2) Cross-Flow filtration cell - round with tangential feed fluid;

3) Cross-Flow rectangular filtration cell.

The working hypothesis in hydrodynamic studies is that optimal conditions can be identified in terms of velocity levels, shear stresses, and field homogeneity at the membrane surface. These conditions are directly linked to the control of membrane fouling and the maintenance of a stable permeate flux.

The working hypothesis in mass transfer studies is that sufficient model predictivity can be achieved. This would enable the simulation of conditions within the concentration polarization layer and provide reliable estimates of mass transfer coefficients near the membrane. The development of mass transfer models for a membrane module represents a contribution to the current state of knowledge in this field. Its significance for formulating innovative engineering solutions lies in the potential to optimize operating conditions of the filtration process, thereby improving both productivity and product quality. Such information is obtained from the spatial and temporal distribution of concentrations in the system, derived from the solution of the model.

2. Objectives

1) Modelling on hydrodynamics on filtration cells with membrane modules, through application on

computerized methodology on computational dynamics (CFD);

2) Determination on the shearers voltages, dynamic pressure and hydrodynamic modes on mixing, depending from the specifics on the specific system;

3) Analysis on available correlations for the odds-on mass broadcasting nearby to semi-permeable membrane, as well as on those predicted from the CFD simulations;

4) Research on mass broadcasting in various constructions on cells for nanofiltration:

- in the boundary layer to membrane surface;
- for the cell as a whole;
- determination on the odds-on mass broadcasting from fluid to the membrane;

5) I will be proposed method for assessment on efficiency on filtration process through key parameters that connect hydrodynamics with the separating process with the aim of determination on the optimal conditions on the process.

6) Comparison of the CFD simulations with experimental one's data.

III. MODEL FOR STUDYING NANOFILTRATION THROUGH COMPUTATIONAL FLUID DYNAMICS

The tasks were solved in a numerical experiment using the ANSYS FLUENT R13.0 software. The software combines tools with a graphical interface, providing setup and solutions for tasks related to real fluid hydrodynamics. The central module (Solver) of FLUENT solves the Navier-Stokes equations under specified boundary conditions and generates information about the hydrodynamic field by setting values for a wide range of hydrodynamic variables for each point of the analyzed volume. With its help, the numerical simulations related to the tasks set in the dissertation were carried out. For this purpose, the workflow is divided into several stages, including: /1/ preparation of an accurate geometric model, /2/ discretization of the volume using the computational grid of cells, /3/ carrying out a computational iteration procedure for numerically solutions the transport equations, /4/ processing and analysis of obtained hydrodynamic solution (Figure 1) [15].

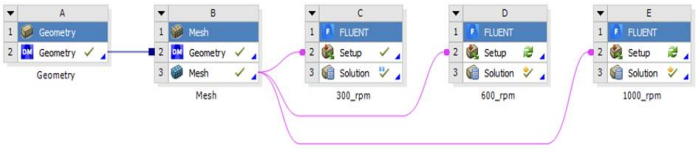

Figure 1. Workflow

IV . CFD STUDY OF FILTERATION CELLS

1. CFD study of an external membrane with permeate flow perpendicular to the membrane surface

Membrane cell with agitator and flat bottom membrane, Dead-End type, i.e. the directions of movement of the fluid and the permeate coincide (perpendicular to the membrane surface).

The proposed numerical model is based on a laboratory membrane nanofiltration cell. MET cell, manufactured by Evonik MET LTD, UK [16]. The cell geometrical model (based on the laboratory cell dimensions) for the numerical simulations had a cylindrical upper section and a conical base section with dimensions 100 mm total height, 46 mm diameter of the upper section and a membrane diameter T = 83 mm. It was stirred by a stirrer with a height 12 mm at a distance of 4.5 mm from the membrane surface. In the experimental module the agitator is a polymer coated magnet rotating in a magnetic field, the base of the cell being placed on the plate of a magnetic device The laboratory model of the cell is located in University of Chemical Technology and Metallurgy, Department of Engineering "chemistry" (figure 2). The geometry of the stirring cell is shown in Figure 3.

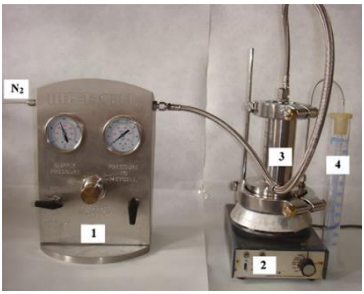

(1) Regulator on pressure;

(2) Magnetic stirrer;

(3) Filter cell;

(4) Measuring cylinder (Permeate).

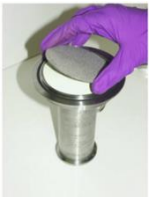

Figure 2. Laboratory model of a flat membrane filtration cell

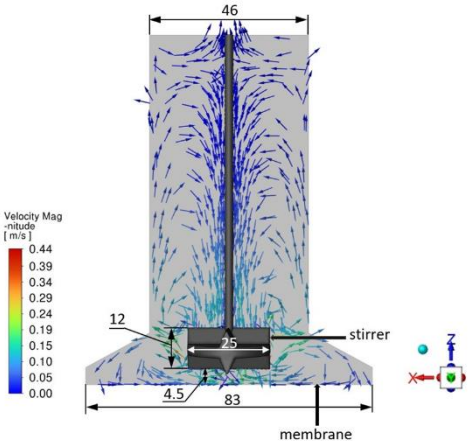

Figure 3. A Dead-end filtration cell: dimensions and flow pattern by velocity vectors (colored by velocity magnitude) at 300 rpm

1.1. Preliminary information from physical experiments to determine the simulation conditions

The dead-end filtration data refer to laboratory cell (MET cell, Evonik MET LTD, UK) with effective surface area *A*=54 cm2, 20bar transmembrane pressure (TMP), working volume up-to 200ml.

The nanofiltration cell provides for a single loading of fluid and filtration to a certain permeate / retentate ratio, followed by reloading. This design is suitable for laboratory studies and is widely used for the initial study of flow and retention behavior for a given system. This periodic operation implies a greater likelihood of fouling and/or clogging of the membrane.

The permeate flux J (L/m ^{2} h) was obtained from the permeate volume V (ml) determined at various times t (s):

$$J = \frac{V_p}{A.t} \quad (2)$$

Flux evolution over the time of filtration J (t) was measured after each 20ml permeate. Membranes resistant to organic solvents were used: Duramem TM (MWCO 300 and 500 Da) and Starmem TM 240 (MWCO 400 Da). The results are illustrated by polyphenols and flavonoids concentration in ethanolic (96%) extracts of: (I) Mursalski tea (aerial parts of cultivated hybrid *Sideritis scardica*×*Sideritis syriaca*); (II) tobacco leaves (*Nicotiana tabacum L.*), (III) *(Hypericum perforatum L. - petals, leaves, buds)* The relevant bioactive compounds in the extracts have molecular weight from 300 to more than 700Da [17].

1.2 Model features and boundary conditions

To create an accurate 3D geometric model, the following sequence was adopted for building a virtual prototype of a membrane filtration cell:

- Construction of the exact geometry of the mixing device. In this case, a method for building the mixer blades and the " Pattern " function for subsequent rotational copying were applied.
- Construction of the disk to the blades and shaft. Simple cylindrical bodies with a given diameter and height are constructed.
- Creating a body that outlines the volume of the vessel. In this case, these are 2 cylinders and a truncated cone between them, with the corresponding heights and diameters.

As a result of the above sequence, an accurate geometric model of a filtration cell with a flat membrane was built (Figure 4).

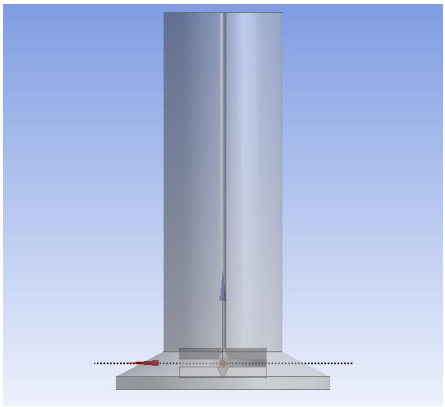

Figure 4. Computer model of DE membrane filtration cell

After the geometric model is formed, the surfaces necessary to set the boundary conditions are determined. This is extremely important because it shows the computational module how to treat the individual geometric figures. For the purposes of the process in this study, the classification is as follows: agitator, shaft and membrane. As a final stage of this

procedure, a tetrahedral mesh is built with an increasing number of elements towards the membrane surface.

The simulations were conducted with two agitator diameters 25 mm and 34 mm. For illustration, the network at a 25 mm agitator diameter is presented in Figure 5.

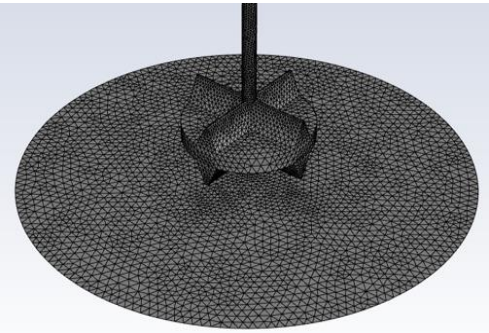

Figure 5. Numerical mesh of the stirred DE filtration cell, containing 959 128 elements.

Figure 6 shows the same configuration with a stirrer diameter of 34 mm.

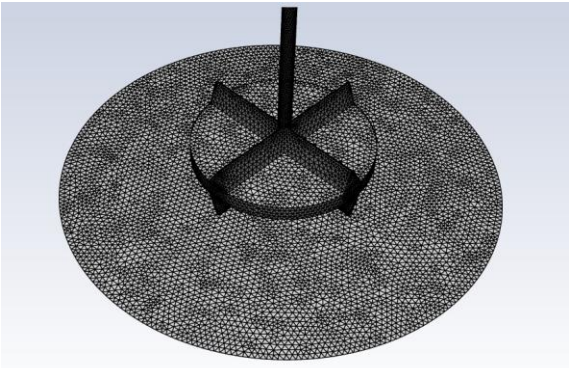

Figure 6. Numerical mesh of the stirred DE filtration cell, containing 1 382 526 elements.

The computational process was set up in several stages using the " Solver " panel. The main parameters related to the calculation methodology are set in it:

- The introduction of turbulence into the transport equations is carried out through models for finding the turbulent kinetic energy k and the rate of its dissipation ε. A realizable k-e model of turbulence was employed
- The calculations were performed using the physical properties of water at 20ºC, which is assumed to be incompressible and isothermal with constant density and viscosity.
- The rotation speed of the stirring device during the experiment was 300, 600 and 1000 rpm, respectively.
- The adopted model of the single moving reference system (Moving reference frame - MRF) [18]allows for a steady-state solution. For a steadily rotating frame (i.e., the rotation rate is constant), it is possible to transform the equations of motion of the fluid to the rotating frame so that steady-state solutions are possible. By default, ANSYS FLUENT allows the activation of a moving reference frame with a constant rotation rate. If the rotation rate is not constant, the transformed equations will contain additional parameters that are not included in the FLUENT formulation.
- For elements classified as walls, the velocity is zero;
- The outlet pressure is set to 0 Pa. This contradicts the physical process of filtration, but the pressure value does not affect the solution of the adopted equations. In the k-epsilon turbulence model, the return flow through the boundary surface is assumed to be turbulent kinetic energy 1 m^2/s^2 and the dissipation rate of turbulent kinetic energy 1 m^2/s^3.
- The computational procedure is initialized by setting specific values for the following variables, characteristic

of the hydrodynamic model, as initial values for the first iteration. The velocity components in the volume x, y, and z are set to zero. The initial turbulent kinetic energy is set to 1 m^2/s^2, and the turbulent kinetic energy dissipation rate is set to 1 m^2/s^3.

- After tests for the independence of the results from the network, a good compromise between the computational time and the deviations of the parameters was found. The convergence criteria are monitored during the computational procedure. It is automatically interrupted when all the specified criteria are met. In the specific studies, a convergence criterion of 1e-05 for all equations in the solved system was adopted.

1.3. Results - velocity distribution, shear stress, mass transfer coefficient in DE filtration

The present study simulates the flow behavior in a DE filtration cell, by revealing the effect of stirrer's speed on the velocity and shear stress distribution at the membrane surface. The rotation of the stirrer induces a strong tangential flow at the DE cell bottom, which swipes the membrane surface and prevents from membrane fouling. The increasing of the permeate flux with increasing of stirrer speed observed from the experiment is connected with the increase of the shear forces at the membrane surface, which enables to control the membrane operation.

Figure 7 shows the shear stresses on the membrane surface at rotation speeds of 300, 600 and 1000 rpm and a stirrer diameter of 25 mm. The same are presented in Figure 8 at a stirrer diameter of 34 mm.

d = 25 mm

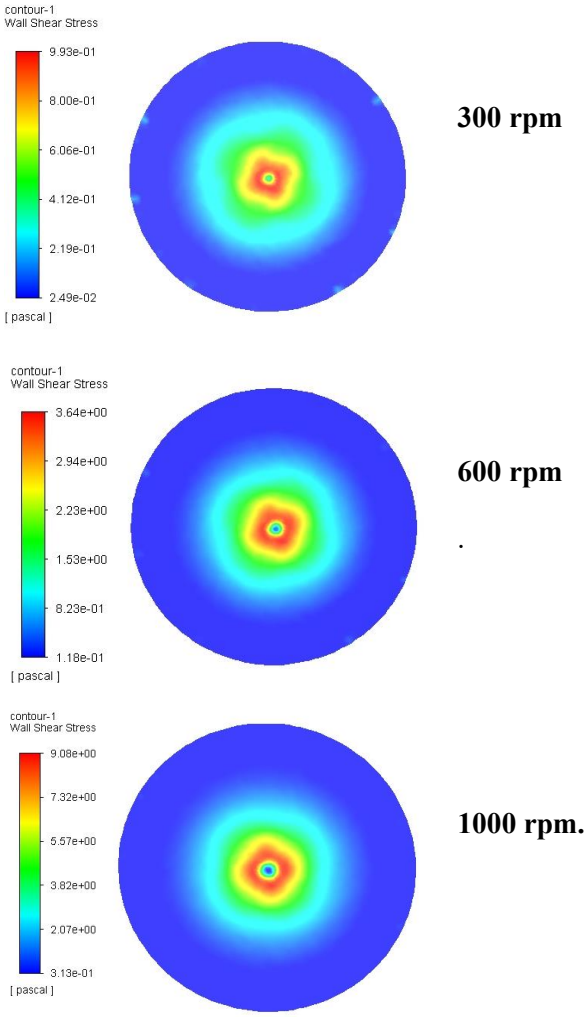

Figure 7. Contour plots of shear stress (Pa) distribution on the membrane surface at stirrer diameter of 25 mm

d = 34 mm

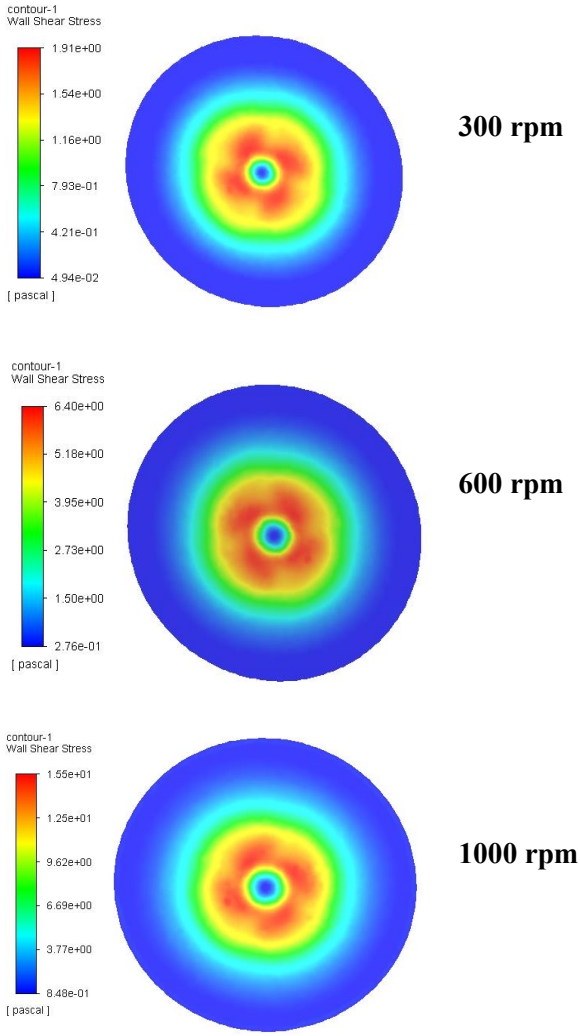

Figure 8. Contour plots of shear stress (Pa) distribution on the membrane surface at stirrer diameter of 34 mm

An increase in the stirrer speed from 300 to 1000rpm leads to 7-fold rise in the calculated average wall shear stress, shown in Figures 9a) and 9b). The evolution of the minimum, mean and maximum shear stress is presented as a function of the stirrer Reynolds number:

$$Re = \left(\frac{\rho N d^2}{\mu}\right), \qquad (3)$$

where N the stirrer speed (s), d is stirrer diameter (m), ρ is the density of the fluid (kg.m^3) and μ is the dynamic viscosity (Pa.s).

The data in Figures 9a) and 9b) correspond well to the measurements by an electro-chemical technique in a DE stirred filtration cell, Koutsou and Karabelas [19], an agitator of the same design and similar dimensions. The reported average membrane shear stress is in the range of 0.8-9Pa at 150-900rpm

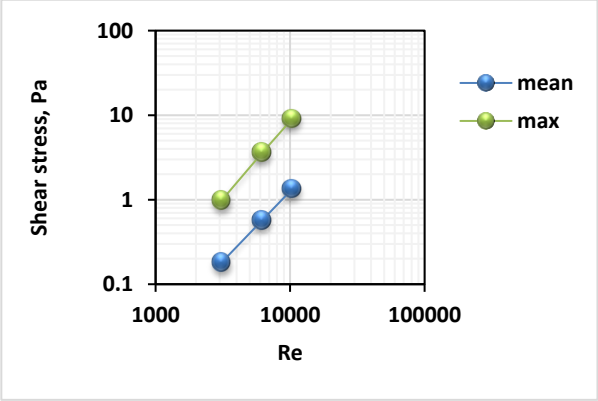

a)

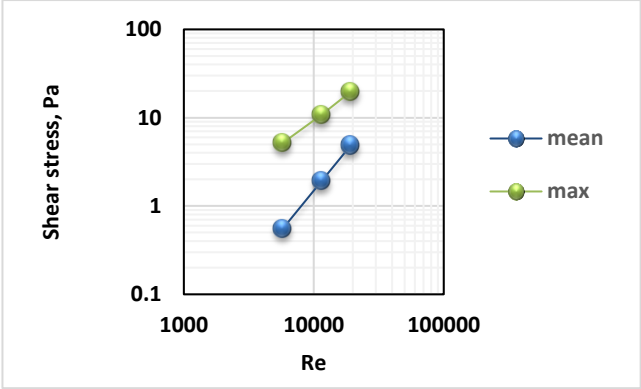

b)

Figure 9. Shear stresses (Pa) versus Re number, Area-weighted mean and maximal a) at a stirrer diameter of 25mm; b) at a stirrer diameter of 34 mm

Figure 10 show the result of the calculations for the maximum and average mass transfer coefficient to the membrane surface.

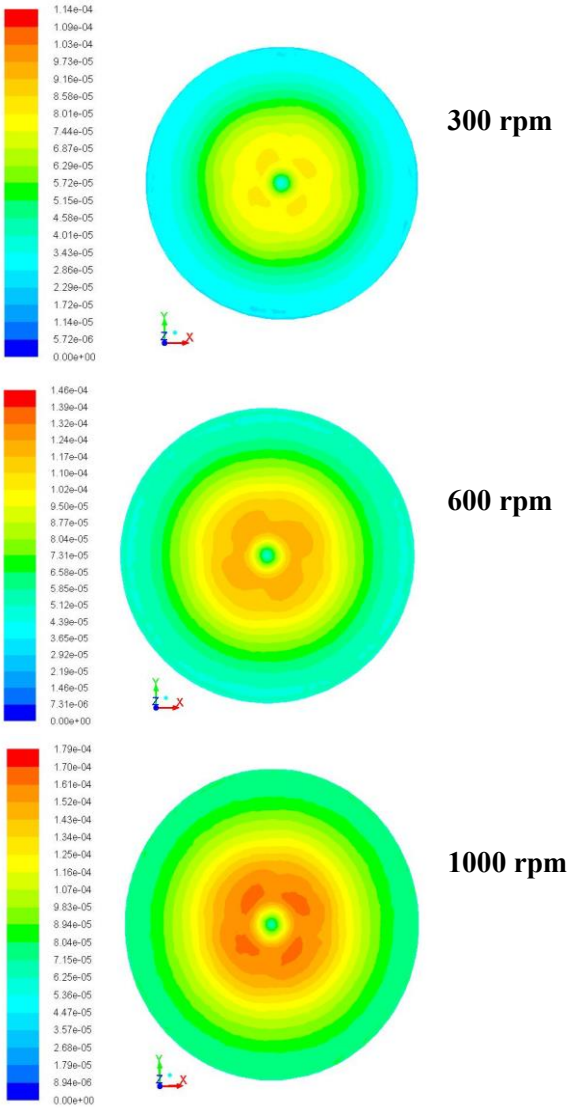

Figure 10. Contour plots of mass transfer coefficient distribution (m/s) on the membrane surface

This work presents a fluid flow simulation of a dead-end (DE) filtration cell including mass transfer modelling using CFD. The effective membrane operation is dependent on the formation of a concentration polarization layer at the membrane surface and membrane fouling, which is controlled mainly by the shear stress and mass transfer coefficient distribution and magnitude at the membrane surface.

The local mass transfer coefficient k_L (m/s) is evaluated from the distribution of the wall shear stress on the membrane surface by using the correlation of Reiss and Hanratty [20] (equation 4). The equation relates the shear rate and the diffusion rate in the boundary layer.

$$k_L = 0.862\left(\frac{\tau D^2}{\mu d_e}\right)^{1/3}, \quad (4)$$

where τ indicates the wall shear stress (Pa), D is the diffusion coefficient ~ $6.7.10^{-10}$ m^2/s and d_e is the sensor diameter (0.001 m).

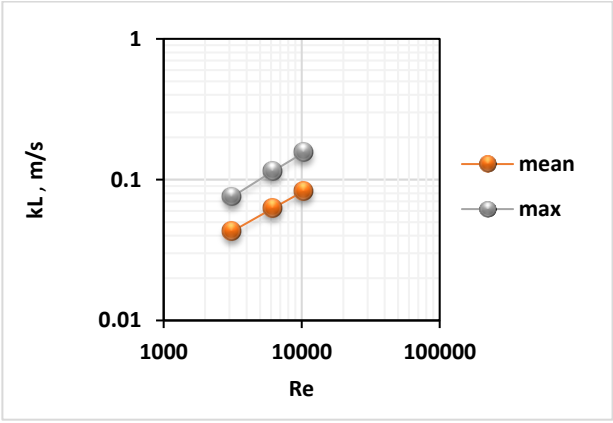

a)

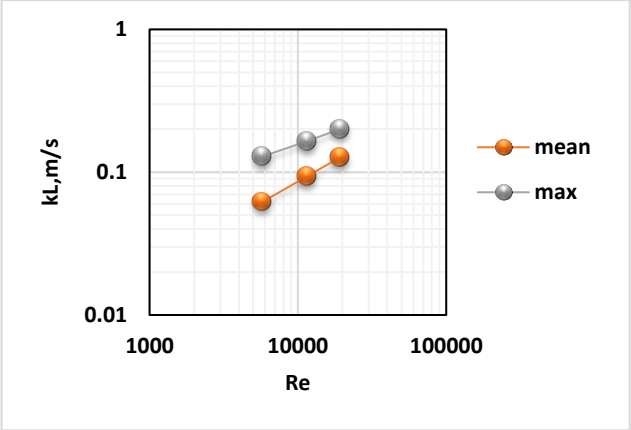

b)

Figure 11. Area-weighted mean and maximal mass transfer coefficient at the membrane surface, m/s x 10 $^{-4}$; a) at stirrer diameter of 25 mm; b) at stirrer diameter of 34 mm

Calculations with a 0.025 m diameter of the agitator show that the smaller diameter leads to a decrease of 67- 72 % in the mean wall shear stress at the membrane and consequently 31-35 % decrease in the mean kL in the range of the rotational speed 300 -1000 rpm, corresponding to Re = 5800 - 19200.

For a specific cell and stirrer geometry the CFD simulations allow visualizing the velocity and shear stress field close to the membrane surface (Figure 12a). They show an uneven shear stress distribution on the surface of the membrane, with values varying within one order of magnitude.

Due to the low ratio of the stirrer to membrane diameter (0.41), a considerable zone of the membrane operates under low fluid velocities, this observation being related to the mass transfer resistance in the adjacent boundary layer. The latter is expected to decrease with increased shear stresses at the membrane surface and can be observed from the velocity distribution to the membrane and the boundary layer thickness. The same figure illustrates the points, where velocity profiles

normal to the membrane are taken. Because of the axial symmetry of the flow, five points along the membrane radius were chosen – two of them lying inside and three - outside the zone of the stirrer (distance from the axis respectively 5.18 mm; 10.37 mm; 20.74 mm; 31.11 mm; 39 mm). The stirring velocity was equal to the one used in the experiments, i.e. 300 rpm. The respective velocity profiles close to the membrane are shown in Figure 12b). They refer to the space under the stirrer (distance 5 mm from the bottom). Moving from the stirrer's axis towards the periphery of the vessel the velocity increases while in the stirrer zone; then gradually decreases, the velocity profiles becoming smoother.

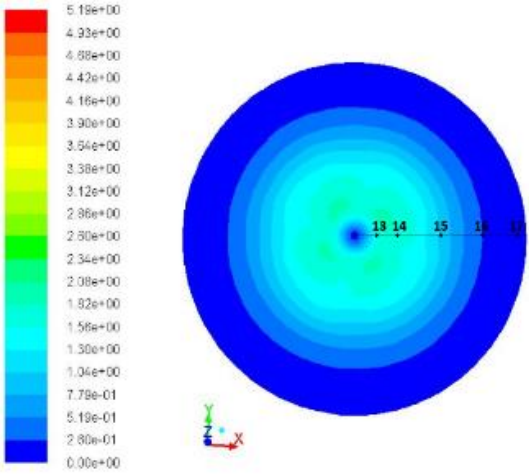

a)

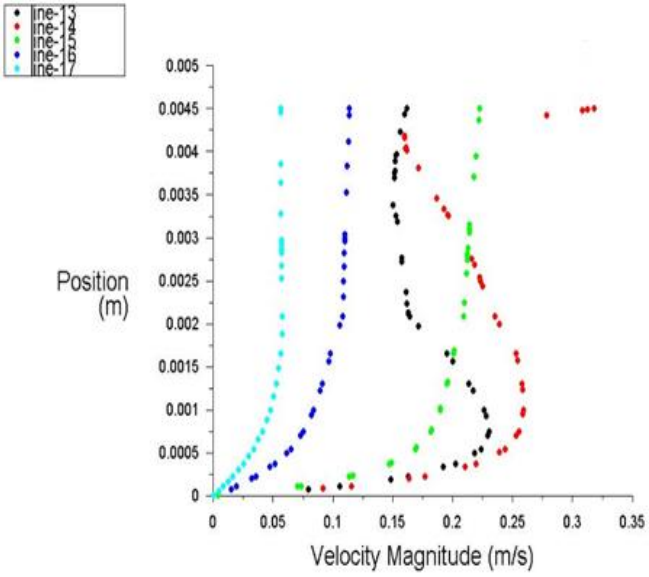

b)

Figure 12. CFD simulations of a) shear stress (Pa) distribution on the membrane surface; b) velocity profiles to the membrane

CFD simulations of the nanofiltration cell show an uneven shear stress distribution on the surface of the membrane, due to unfavorable stirrer to membrane diameter ratio. (=0.41). The latter is important for the mass transfer resistance in the adjacent boundary layer, which is expected to decrease with increasing shear stresses at the membrane. Thicker boundary layers and high rejection coefficients favor the concentration polarization influence. The boundary layer thickness, determined by the zone with higher velocity gradient of each profile, gives values between 60 and 430 mm for the above mentioned five points, with an average value of about 250 mm for the membrane as a whole.

These results also support the need for the aforementioned mathematical model accounting for concentration polarization,

as it manifests itself more strongly in the presence of a thicker boundary layer and high retention coefficients at the membrane.

Conclusions:

The mass transfer coefficient, calculated in accordance with the concentration polarization theory, is comparable with the reported values for natural antioxidants such as polyphenols.

The study allows to calculate and predict the importance of concentration polarization in the separation of polyphenols by nanofiltration as well as to improve the process conditions

2. CFD study of an external cylindrical cell with permeate flow tangential to the membrane surface (CF)

A MET cell (Membrane Cell) cross-flow system was used. Extraction Technology Ltd., UK, with four series-connected flat sheet cells (membrane area 54 cm ^{2}) at a constant cross-flow rate of $2x10^{-5}$ m^3/s and a transmembrane pressure of 20 bar. The filtration cell is a flat cylinder 5 mm high, with a membrane at the bottom of the base with a diameter of 83 mm (Figure 13).

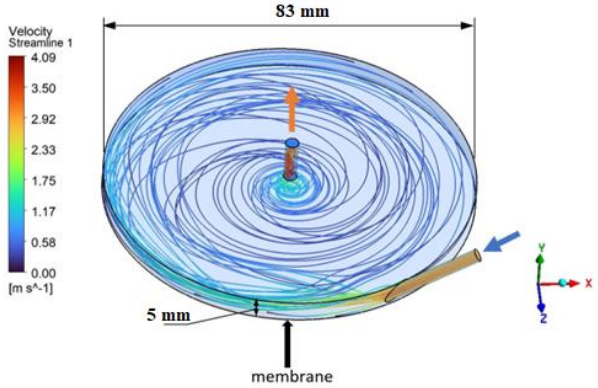

Figure 13. Cross-flow filtration cell: dimensions and cross-flow streamline (colored by velocity magnitude) at Qf =2x10-5 m3/s

As can be seen from Figure 13, this cell is flow-through, with the inflow and outflow illustrated in the figure.

2.1. Preliminary information from physical experiments to determine the simulation conditions

The simulated cross-flow cell is taken from a study on concentration of polyphenols from ethanolic extract of Mursalski tea (*Sideritis ssp*.). A Duramen 500 membrane was used, details of the experimental setup are presented in [21]. The membrane was pre-adapted with the solvent. The permeate flux J (L/m ^{2} h) was obtained from the permeate volume V (ml) determined at various times t (s) - (equation 2).

The solution enters the cylindrical cell tangentially through the surrounding wall of the cylinder and leaves the cell at the center of the upper base, providing turbulent hydrodynamic conditions (Figure 14). The membrane area is 54 cm² in tangential Cross-Flow mode, i.e. the directions of movement of the fluid and the permeate are mutually perpendicular.

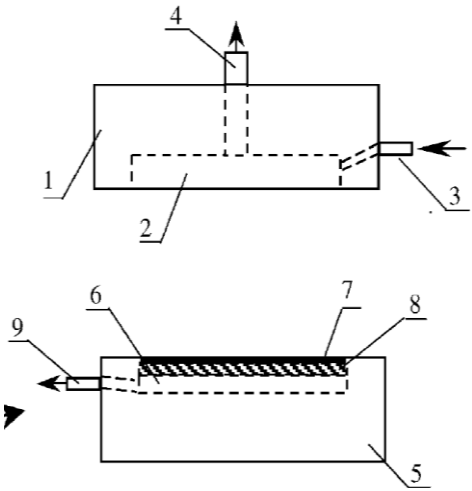

1. Lid
2. Retentate channel
3. Solution inlet
4. Permeate outlet
5. Bottom
6. Permeate channel
7. Membrane
8. Sintered disc
9. Permeate outlet

Figure 14. Scheme of an external circular CF membrane cell

2.2 Model features and boundary conditions

The geometric model is shown in Figure 15. The height of the retentate channel is 5 mm, and the diameter of the inlet and outlet is $d_{in/out} = 3$ mm, the cell diameter is $D_{cell} = 83$ mm. The tangential feed inlet results in rotational turbulent flow in the cell, which ensures stable operation, by reducing concentration polarization and preventing from membrane fouling. The concentrate outlet is in the centre of the cell top. The cell bottom represents a membrane

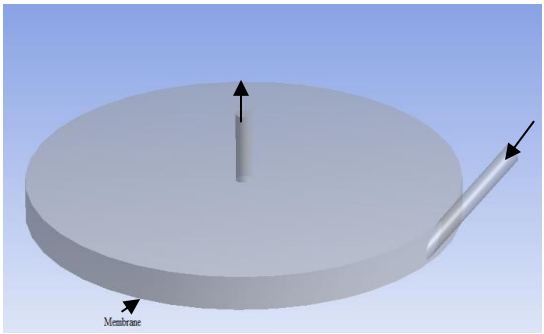

Figure 15. 3D geometric model of a circular CF filtration membrane cell with tangential fluid supply

The mesh of the 3D calculation domain is tetrahedral, allowing refinement near the surface of the membrane - figure 16 and contains 809 293 cells, cells was found appropriate for mesh independent results.

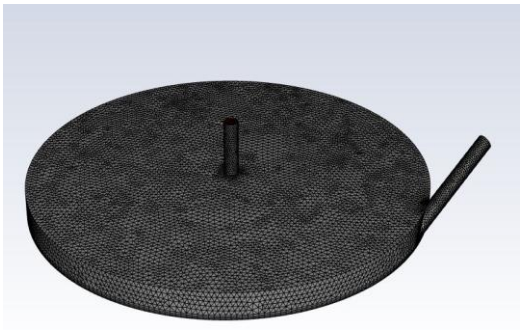

Figure 16. Numerical mesh of the stirred CF filtration cell, containing 809 293 cells

The computational process is set up in several stages via the “Solver” panel:

- The “Realizable k-ε model” model of turbulence;
- The used liquid is water with constant physical - chemical properties;
- The speed on feed is 1.58, 2,83 and 5.90 m /s, at debit Q_f = 0.7 - 2.5 l/min;
- The boundary condition for the pressure output is (p = 0);
- All remaining hard walls on the vessel (membrane, wall-solid) are asked as boundary condition type wall no-slip;
- For each solution, convergence was monitored continuously. In the specific studies, a convergence criterion of 1e-04 was adopted for all equations.

2.3. Results – velocity distribution, shear stress, mass transfer coefficient in CF filtration

Figure 17 presents the shear stresses on the membrane surface at a flow rate Q_f = 2.5 L/min.

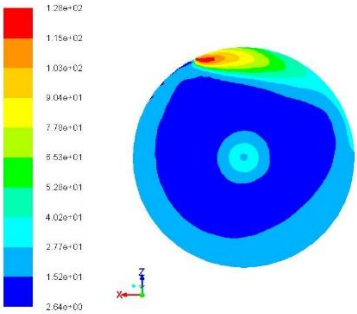

Figure 17. Contour plots of shear stress (Pa) distribution on the membrane surface at Q_f = 2.5 L / min

The tangential orientation of the feed inlet results in a swirling flow within the cell that sweeps across the membrane surface and provides tangential flow with no moving parts near the membrane, as illustrated by the flow lines in Figure 18.

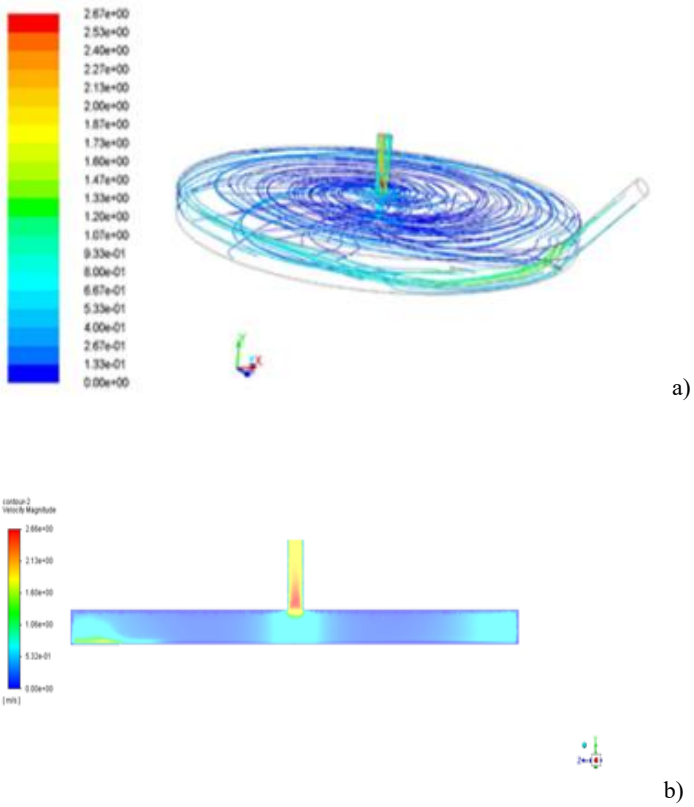

Figure 18. Velocity distribution (m/s) at a) the flow lines of the flat circular cell; b) a plane perpendicular to the membrane

The average shear stress versus feed flow rate - Figure 19 - is compared with experimental data showing the increase in permeate flux with increasing feed flow rate - Figure 20. The comparison confirms the relationship between the increase in permeate flux and the shear forces at the membrane surface, which leads to a decrease in concentration polarization.

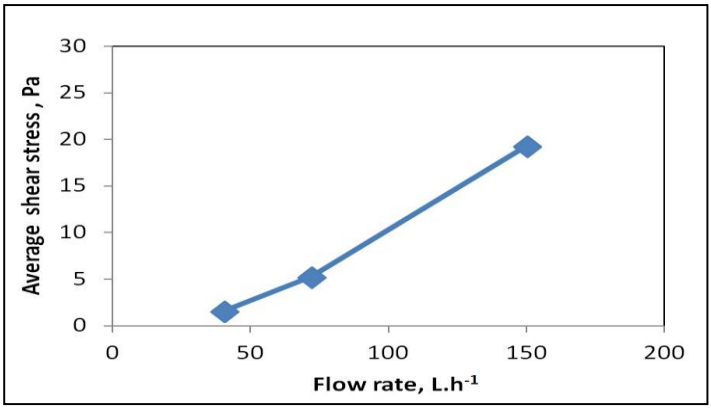

Figure 19. Average shear stress (Pa) versus feed flow velocity (m/s)

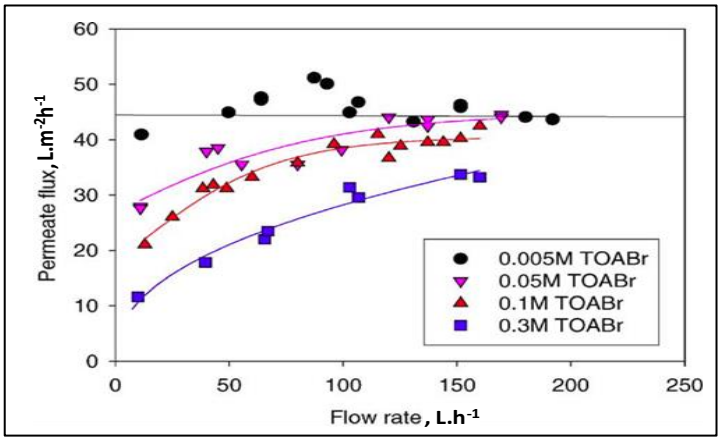

Figure 20. Experimental data from the literature on permeate flux dependence on feed flow rate at different TOABr concentrations in toluene solutions

The mass transfer coefficient on the membrane surface is calculated by equation (4) and shown in Figure 21. At flow rate Q_f = 1.2 L/ min, Schmidt number Sc = μ / D_ρ = 1.5 x 10^3 and constant solution properties, μ = 0.001 kg/m.s. The distribution seems quite regular, with the exception of small regions of high values at the periphery and the centre of the membrane, corresponding to high shear stress.

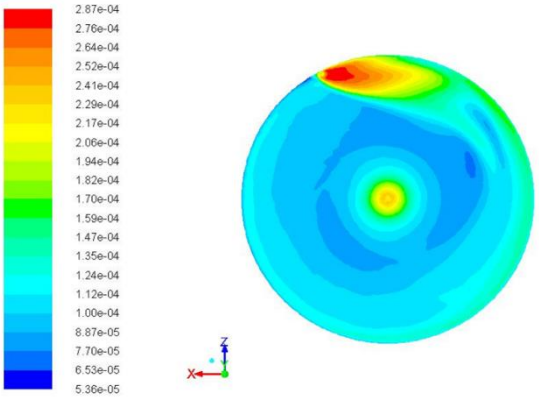

Figure 21. Color contours of the mass transfer coefficient distribution (m/s) on the membrane surface, Q_f=1.2 l/ min, Sc =1.5X10 , Re =28300

For the visualization of the concentration distribution and the concentration boundary layer, simulations are performed at *Sc* = 10 because the small dimensions of the concentration layer at the typical in filtration Schmidt number *Sc* ~ 10^3 need very fine mesh close to the membrane surface and much more computational time. The concentration boundary layer is about 1/10 of the viscous sublayer at typical conditions of cross-flow filtration (Reiss and Hanratty, 1963) [20].

Figure 22 a) illustrate the concentration boundary layer at the membrane surface. As seen in Figure 22b, the boundary layer thickness is smaller at higher velocity in the peripheral zone. In the case shown in Figure 22c of smaller Reynolds

number (*Re*), due to higher viscosity, the boundary layer is much thicker and regular.

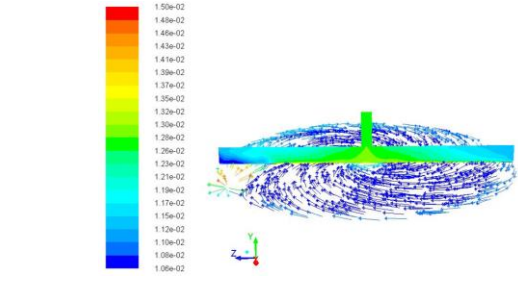

a)

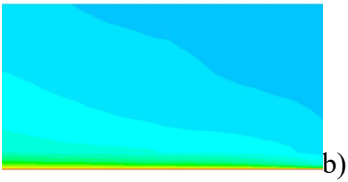

b)

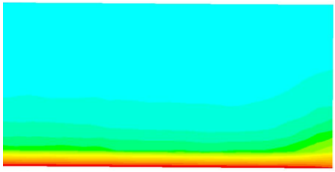

c)

Sc =10, Re =28300 Sc =10, Re =283

Figure 22: Contour plots of mass fraction c (kg/kg) at the mid-vessel plane, Sc = 10, $Q_f = 2 \cdot 10^{-5}$ m^3/s with velocity vectors in the vicinity of the membrane, coloured by velocity magnitude v (m/s)

The space-average Sherwood number (Sh) is calculated by the correlation for turbulent flow in a pipe from Chilton-Colburn analogy [21]:

$$Sh = 0.023 Re^{0.8} Sc^{0.33} \quad (5)$$

where *:*

$$Sh = \frac{K_L d_h}{D} \quad (6)$$

and

$$Re = \frac{v_f d_h}{v} \quad (7)$$

Here k_L denotes the average mass transfer coefficient (m/s), v_f is the feed inlet velocity (m/s), d_h indicates the flow hydraulic diameter (m), and $v = 1x10^{-6}\ m^2/s$ is the kinematic viscosity. In order to determine the hydraulic diameter, it is assumed that the fluid movement in the cell resembles flow in a spiral channel. Since the cell height h is much smaller than its diameter, the hydraulic diameter is calculated by $d_h = 2h$, which is accepted for large flow aspect ratio width to height. The equation has been successfully used in [21] for OSN in a cross-flow cell with the same configuration, but larger membrane surface area (78 cm^2). A comparison of our results for k_L with data from literature sources is presented for reference in Table 1.

Table 1. Comparison of calculated mass transfer coefficient (m/s) with reference data

Author	*Qf* (l/min)	Inlet speed v_f (m/s)	Volume average cross-flow speed v_{va} (m/s)	*Re* x10 $^{-4}$	*Sh*	k_L x 10 ^{5} (m/s)
This study , *Sc* =1500						
	0.7	1.58	0.57	1.58	586	3.93
	1.2	2.83	0.25	2.83	934	6.26
	2.5	5.90	1.70	5.90	1680	11.3
Peeva and al . (2004)						
	0.7 - 1.3					0.6 - 1.9
	2 - 2.5					1.7 - 5.3
Koutsou and Karabelas (2012) *Sc* =2025					500-950	2 - 11

It can be seen that the values of the average mass transfer coefficient k_L are comparable to the data of other authors. It should be noted that the lower values of the mass transfer coefficient, reported in [21] are obtained for higher viscosity of the systems investigated there and bigger dimensions of the filtration cell, leading to lower cross-flow velocity.

Table 1 shows a good agreement of the present results with the electrochemical measurements in [19], in a dead-end filtration cell with stirring.

Conclusions:

The calculated values of local and average mass transfer coefficients are comparable with the available reference data from literature sources. The picture of the local mass transfer coefficient obtained corresponds to the particular membrane shear stress distribution and is related to similar input parameters, such as cross flow velocity and system physicochemical properties.

The tangential orientation of the feed inlet results in cell-contained swirling flow that sweeps the membrane surface and ensures tangential flow near the membrane, eliminating the need for in-built mobile components. The circular turbulent flow is favorable for high membrane shear stress, preventing fouling.

The increase in the mass transfer coefficient with cross-flow velocity, in agreement with experimental data, confirms the relation of the increase in the permeate flux with the reduction of the concentration polarization layer.

3. CFD study in a rectangular filtration cell

3.1. Preliminary information from physical experiments to determine the simulation conditions

A laboratory membrane filtration unit (MaxiMem, Prozesstechnik GmbH) with a rectangular flat-sheet membrane of 215 cm^2 active area was operated at different pressures (5–20 bars) and cross-flow rates (CFR 50−125 L/h). [22], is shown in Figure 23. The laboratory model of the cell is located in Institute of Solid-State Physics at the Bulgarian Academy of Sciences.

Figure 23. Rectangular external filtration cell

3.2. Model features and boundary conditions

CFD modeling (FLUENT code) is focused on determining the shear stress along the membrane surface.

An accurate 3D geometric model of a rectangular extended membrane cell is presented in Figure 24. The model was built in the Ansys environment. Design Modeler. After shaping the geometric model, the surfaces necessary to set boundary conditions (inlet, outlet, membrane) are defined.

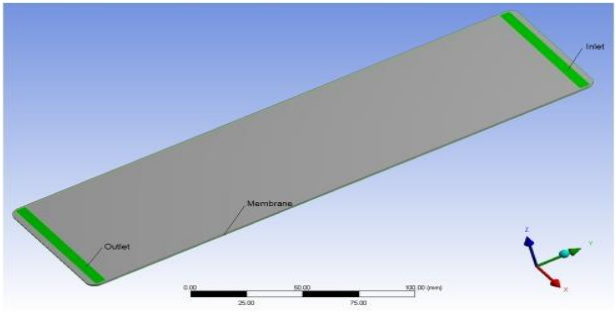

Figure 24. 3D geometric model of a rectangular extended membrane cell

The 3D computational domain mesh is tetrahedral, allowing for densification near the membrane surface. It contains 1 129 587 elements, shown in Figure 25. The analysis of the dependence of the results on the number of cells was performed in order to select a mesh that achieves high accuracy of the results and optimal calculation time.

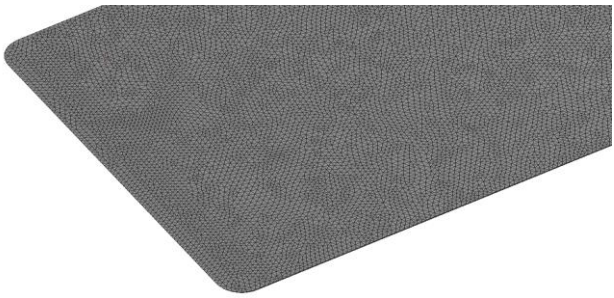

Figure 25. Numerical mesh of the stirred DE filtration cell, containing 1 129 587 elements

The calculation process is set up in several stages through the "Solver" panel. The main parameters related to the calculation methodology are set in it.

- The calculations were carried out taking into account gravity and the physical properties of water at 20ºC and atmospheric pressure;
- Steady-state flow was assumed in the 3D computational domain under laminar regime (Re = 260–660) corresponding to the experimental conditions in the cell. These assumptions are supported by the operation of the NF cell in cross-flow mode with constant flow rate, the permeating flow rate through the membrane (0.21–0.43 L/h) being negligible when compared to the cross-flow one (50–125 L/h);
- The velocity indicated at the inlet (0.034, 0.051, 0.068, 0.085 m/s). Velocity was specified at the inlet; its value

was in accordance with the range of CFR used in the experiments and the particular geometry (cross section area) of the cell inlet;
- At the outlet, a pressure outlet boundary condition was assumed (p = 0);
- No-permeation and no-slip conditions were set at the membrane wall;
- In the specific studies, a convergence criterion of 1e-04 was adopted;
- Impermeable membrane.

3.3. Velocity distribution, shear stress and mass transfer coefficient in CF filtration

This study considers the effect of cross-flow velocity and transmembrane pressure on flux and rejection behavior during nanofiltration. Along the cell a higher intensity of the shear stress is observed in the upper part (accounting for the vertical position of the cell and downward motion of the fluid) i.e. close to the feed channel, - figure 26. This observation is confirmed by the membrane surface itself after filtration. A picture of the latter is shown in figure 27.

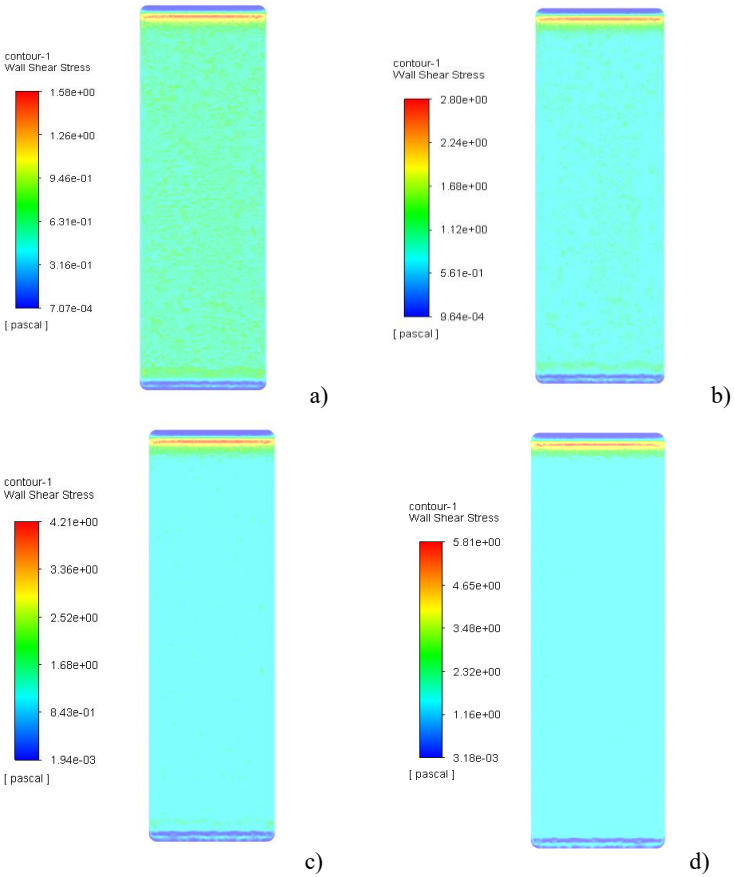

Figure 26. Contour plots of shear stress (Pa) distribution on the membrane surface, at tangential velocity a)0.034, b) 0.051, c)0.069, d) 0.086 m/s

Figure 27. Photo of the membrane surface after nanofiltration

Figure 28 presents the velocity distribution through colored contours at different flow rates.

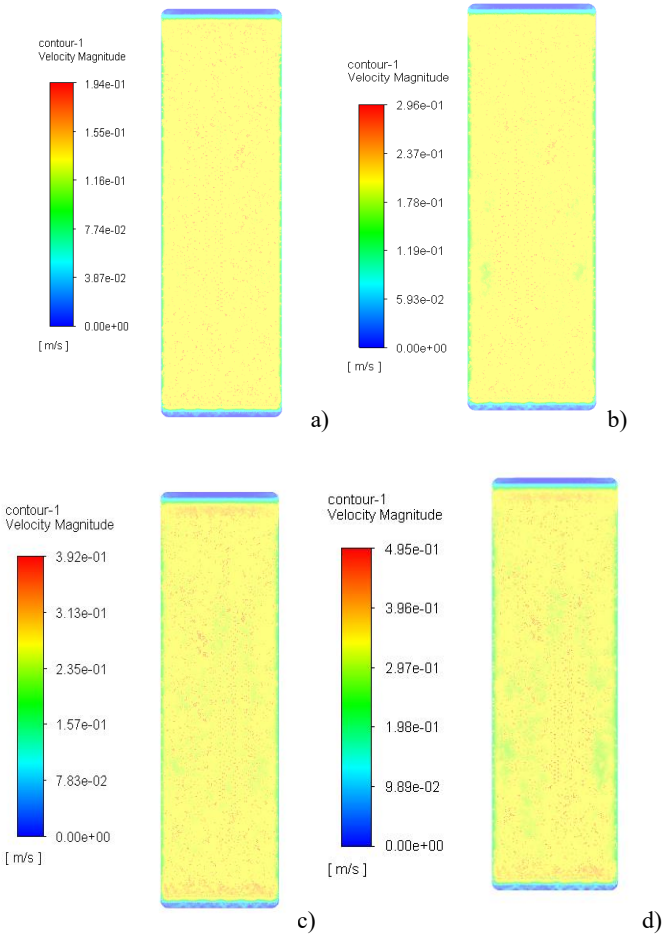

Figure 28. Contour plots of velocity magnitude (m/s) on the mid-vessel plane at a distance of 1 mm, at tangential velocity a)0.034, b) 0.051, c)0.069, d) 0.086 m/s

The effect of higher CFR is found in inhomogeneity of the shear stress distribution at the membrane, i.e. the maximum shear stresses enhance faster than the respective minimum and

mean averaged values. The results of the CFD simulations – range of velocity and shear stresses, as well as the homogeneity of the latter around the membrane – can be related (though qualitatively) to the experimentally observed insignificant effect of concentration polarization and fouling, i.e. the hydrodynamic conditions in the cell are considered favorable for NF treatment of this multicomponent system, in which the three groups of components were targeted. A 2.5-fold increase of the CFR leads to a 3.7-fold higher calculated maximum shear stress, while the mean surface averaged values increase 2.7 times. These results are illustrated in Figure 29.

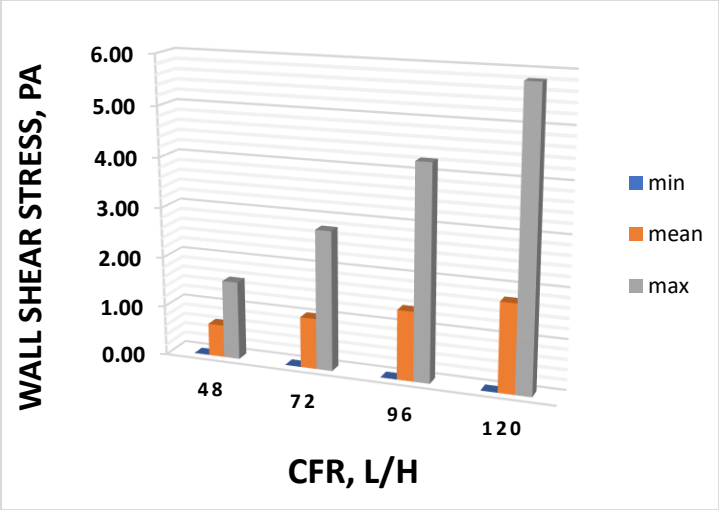

Figure 29. Shear stresses (Pa) vsersus tangential flow rate (CFR)

Conclusions:

The CFD simulation revealed the flow pattern in the filtration cell and a uniform distribution of the wall shear stress over the whole membrane surface. This result confirmed the

good conditions, in terms of fouling control and concentration polarization, in the considered modes of operation.

4. Comparative analysis of CFD simulation results of nanofiltration in DE and CF filtration modes

Our results regarding the behavior of the permeate have been processed. flow over time in nanofiltration with two types of cells (DE and CF) to analyze the hydrodynamic environment around the membrane surface, which is directly related to the phenomena of membrane fouling/clogging and subsequent reduction of the permeate flux. In the practice of membrane separation, semi-empirical models are used to describe the kinetics of this process. In the case of natural extracts, these models prioritize the mechanism of sediment deposition on the membrane surface. The concentration profile at the membrane surface, which is directly related to the phenomena of concentration polarization, depends on the instantaneous value of the permeate flux. In these cases, the hydrodynamic field around the membrane plays a significant role in preventing these processes. The CFD approach used in the dissertation has a great advantage, allowing us to see the distribution of velocities and concentrations and the related calculations (shear stresses, mass transfer coefficients) in the context of a specific membrane cell or submerged membrane reactor design.

In the present work, the hydrodynamic model is for a flat filtration cell with normal and tangential flow to the membrane (DE, CF). In the second case, the calculations were performed for two different cell geometries and flow introduction methods. The obtained shear stresses, averaged over the membrane surface (distance 1 mm) were processed as a function of Re of the mixer (for the DE cell) and Re of the surrounding fluid (for the CF cell). The spatial distribution of the local mass transfer coefficients provides information about the distribution of the efficiency coefficient E_{ff} over the

membrane surface. The membrane surface-averaged value of E_{ff} is an important characteristic that depends on the reactor's operating conditions: Reynolds number, apparent viscosity, and aeration rate.

The rotation of the agitator causes a strong tangential flow in the cell, which slides on the membrane surface and prevents its fouling. The increase in permeate flux with increasing stirrer speed, as observed in the experiment, is associated with an increase in shear forces on the membrane surface, allowing for control of its operation.

The increase in the rotational speed is one of the main measures to control the mem-brane fouling. It results in an increase in the wall shear stress at the membrane surface, and not so substantial increase in the mass transfer coefficient (equation 3). The effect of the rotational flow speed over the membrane surface is demonstrated in Figs 30 and 31.

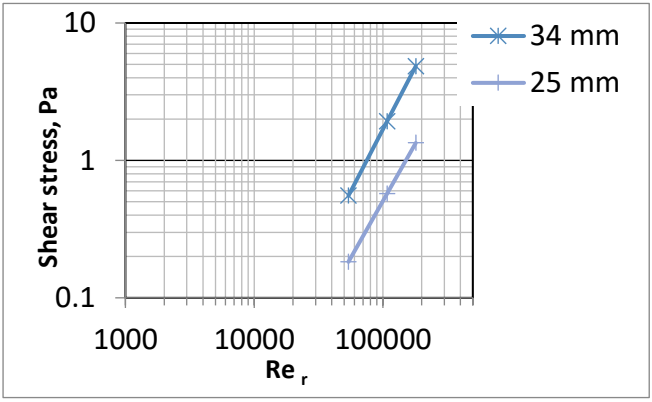

Figure 30. Area-weighted mean shear stress (Pa) at the membrane surface for d=25 mm and d = 34 mm

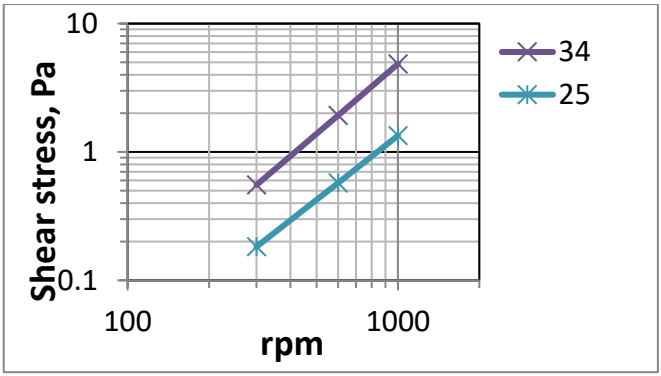

a)

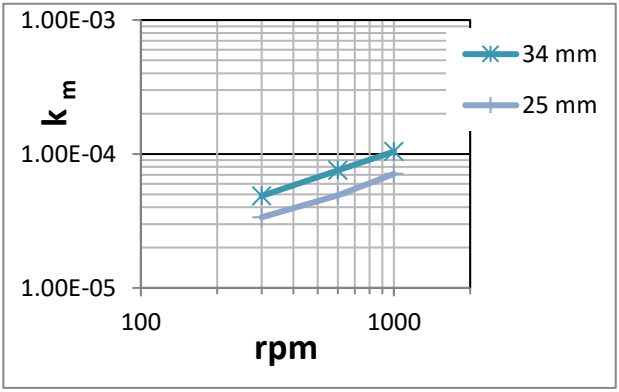

b)

Figure 31. (a) Area-weighted mean shear stress τ (Pa); (b) Mass transfer coefficient km (m/s) at the membrane surface for d=25 mm and d = 34 mm

The results for the case 1 of the smaller stirrer with d = 25 mm compared to the case 2 with d = 34 mm show a substantial decrease in the mean area-weighted wall shear stress at the membrane of about 67% difference (for rotational speed 300 - 1000 rpm), Fig.31a. The bigger stirrer diameter is important mainly for ensuring conditions of high shear stress at the membrane, favorable for control of concentration polarization and stable filtration process but the effect on the mass transfer

coefficient is not so substantial. Due to the relation in Eq. (4), according to which at constant physical properties the respective decrease in the mean area-weighted mass transfer coefficient with the small stirrer is with smaller difference of about 37% (Fig. 31b).

The obtained distribution of k_L over the membrane surface (figure32) at d = 34 mm, N = 1000 rpm shows that the highest value $k_{max} = 1.55x10^{-4}$ m/s is achieved at a radial distance $r = r_c$ close to the agitator tip. The maximum value of the local mass transfer coefficient, achieved under these conditions, can be taken as the highest achievable mass transfer rate for the filtration cell. The filtration efficiency, presented in Figure 33, is calculated as the ratio of the mass transfer coefficient, weighted by the membrane area average value, to $k_{max} = 1.55x10^{-4}$ m/s (Eq. 1).

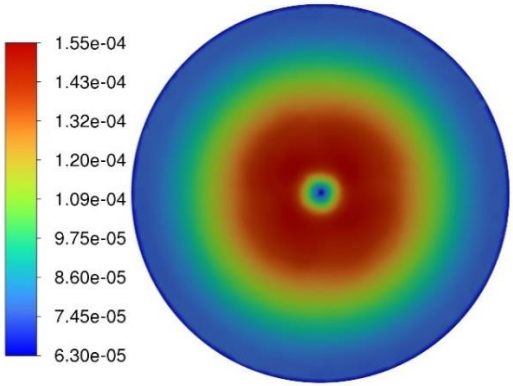

Figure 32. Contour plots of the local mass transfer coefficient distribution k_L (m/s) over the membrane surface at 1000 rpm and d=34 mm

Higher mass transfer effectiveness (E_{ff}) is obtained at higher rotational speeds and greater stirrer diameter, which is demonstrated by the plots in Fig. 33. The increase in the effectiveness at 1000 rpm compared to that in 300 rpm is about

2 times. The increase in the effectiveness at d=34 mm, compared to the case at d=25 mm is about 1.5 times.

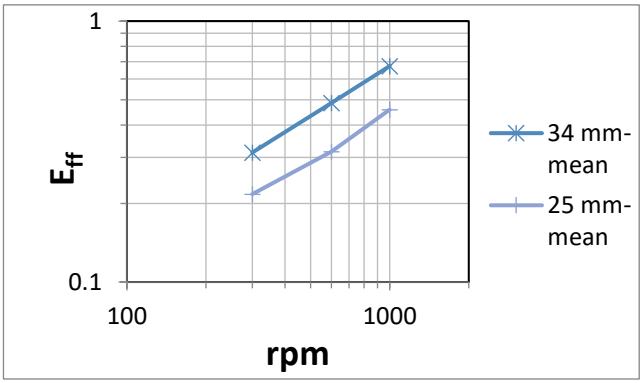

Figure 33. Mass transfer efficiency in a DE filtration cell versus stirrer speed (rpm)

The increase on the stream on permeate with increasing on speed on the mixer, observed from experiment, is associated with the increase on the forces on shearing on the surface on the membrane, which allows yes is controls the work on the membrane. Known are several criterions for comparison of DE and CF modes:

- equality of Reynolds numbers in the two membrane cells, calculated with the diameter and peripheral speed of the agitator (DE) and, respectively, the tangential flow velocity and hydraulic diameter of the cell (CF);
- uniform shear stresses averaged over the membrane surface;
- mass transfer coefficients averaged over the membrane surface.

The resulting dependencies, following each of these criteria, differ, which is why experimental confirmations are an indispensable part of the study.

The comparison between the two regimes provides guidance on the required rotation speed in the DE cell to accommodate certain shear stress conditions in the CF cell. In practice, this compliance usually moves from small-scale DE (laboratory studies) to CF with a transition to larger membrane sizes, as this is the operating regime of industrial membrane modules.

The resulting spatial distribution on the local odds on mass transfer in DE filtration (figure 34) and CF filtration (figure 35), gives information for the distribution on E_{ff} by the surface on the membrane - figure 36 and figure 37.

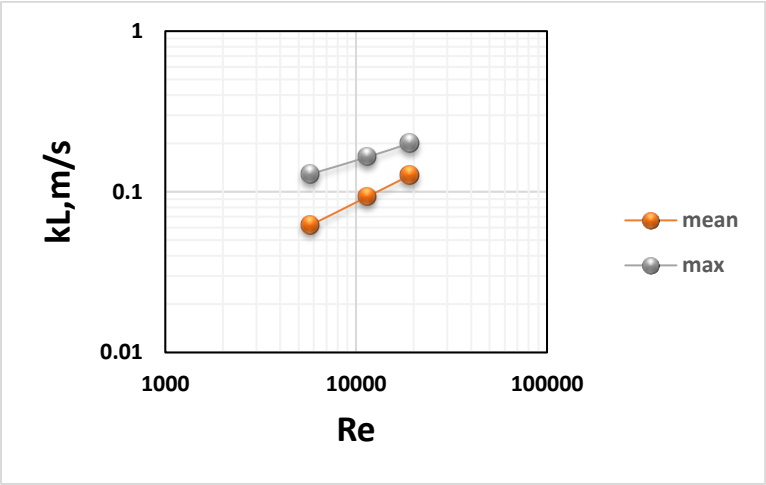

Figure 34 . Area-weighted mean and maximal mass transfer coefficient at the membrane surface, m/s x 10 $^{-4}$ to membrane surface at DE filtration relative versus Re number

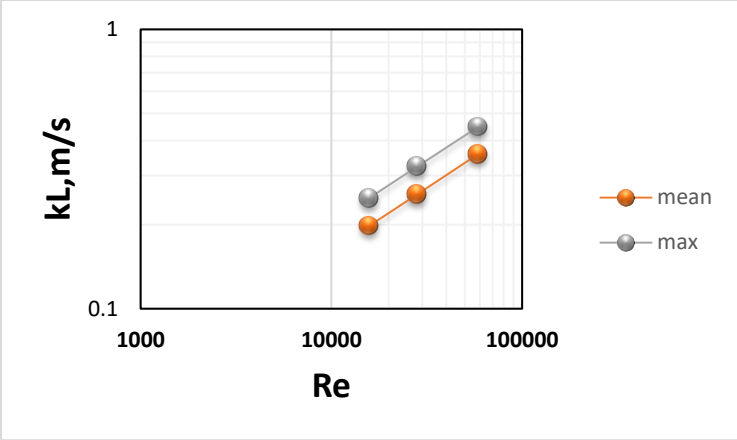

Figure 35. Area-weighted mean and maximal mass transfer coefficient at the membrane surface, m/s (m/s) x 10 $^{-4}$ at CF filtration versus Re number

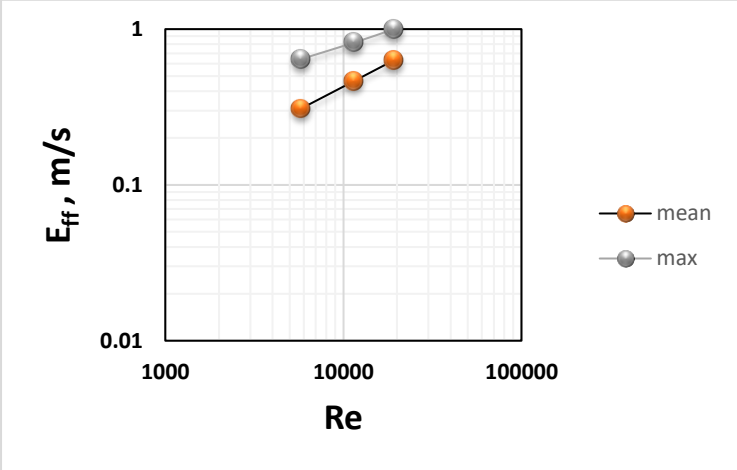

Figure 36. Mass transfer effectiveness in CF filtration cell versus Re number

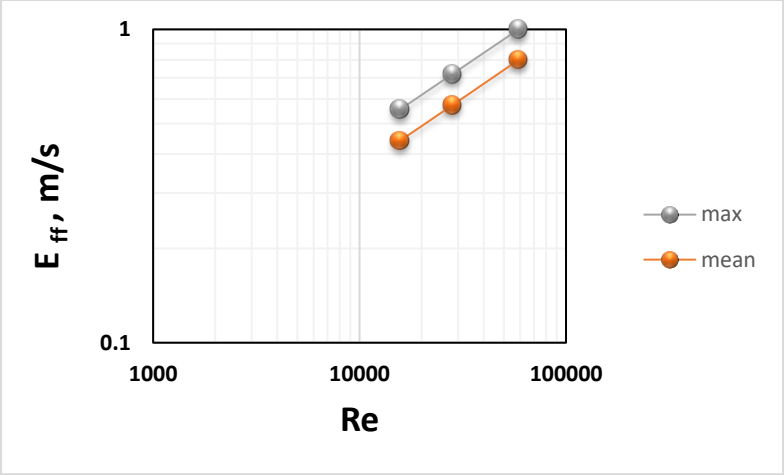

Figure 37. Mass transfer effectiveness in CF filtration cell versus Re number

Membrane cells are usually tested in advance by the manufacturer and a recommended value or range is given for the volumetric flow rate of the fluid through the cell (for CF) or for the speed of the stirrer (for DE). The data shown in the figure correspond to these ranges of values. In the literature, the CF cell is considered to have advantages, which is also visible in the presented figure, where the values shown for the CF cell lie higher and the deviation between the maximum and the average value is smaller, i.e. we have a better and more homogeneous mass transfer along the membrane.

The comparative analysis between the DE and CF operating modes provides valuable information for optimizing the hydrodynamic parameters in the studied filtration cells. At a stirring speed of 1000 rpm in the DE cell and a speed of 5.90 m/s in the CF cell, a general range of Reynolds number values between 15 768 and 19 228 is demonstrated, which corresponds to a similar hydrodynamic regime.

V. CONTRIBUTIONS

The contributions in this dissertation are related to membrane integrated bioreactors and are aimed at a wide range of industrial applications. The main results presented in the dissertation were obtained by computational fluid dynamics modeling, based on previous experience with concentration of antioxidants, such as polyphenols and flavonoids, from natural product extracts by nanofiltration. The numerical study uses the ANSYS FLUENT tools, based on the finite volume method, to numerically solve the Navier- Stokes equations.

1. Evaluation of the influence of the hydrodynamic picture and shear stress distribution in membrane filtration processes using computational fluid dynamics

- The knowledge on membrane separation/concentration by tangential nanofiltration for concentration of biologically active compounds in extracts of medicinal plants with organic solvents has been supplemented. The influence of two factors – solute concentration and tangential flow velocity, which are closely related to concentration polarization in tangential nanofiltration, has been analyzed.
- The experimental approach is complemented by numerical techniques to evaluate the role of the cross-flow pattern in the cell. The velocity and shear stress distribution on the membrane surface was obtained through CFD simulations. The calculations allow determining a range of speeds and voltages representing a compromise between minimal membrane clogging on the one hand and minimal stress/damage to the cell mass in the volume of a stirred membrane bioreactor.

2. Description and prediction of mass transfer in membrane filtration processes using CFD

- The CFD simulation reveals the concentration distribution in the feed channel. It complements previous flow model data with new knowledge of mass transfer aimed at understanding and controlling the concentration polarization phenomenon. The obtained results are analyzed in accordance with the available experimental data.
- mass transfer in a filtration cell with normal flow and mechanical agitation has been supplemented, and through CFD simulations the local velocity profiles, the boundary layer thicknesses and the distribution of local mass transfer coefficients have been clarified, which allows a better understanding of the mechanisms determining the concentration polarization. The conclusions from them find indirect support in the experimental observations in the literature, including our own studies with nanofiltration of natural extracts.

3. Performance evaluation method

- The developed method for assessing the transfer efficiency in integrated processes in a membrane separation bioreactor is based on the use of the potential of CFD simulation and the relationship between the hydrodynamic picture in the reactor and the conditions for mass transfer through the membrane. It has a wide potential for comparative analysis of different design solutions.

Literature

[1] A. Boyle-Gotla, PD Jensen, SD Yap, M. Pidou, Y. Wang, and DJ Batstone, “Dynamic multidimensional modeling of submerged membrane bioreactor fouling,” *Journal of Membrane Science,* vol. 467, pp. 153-161, 2014. https://doi.org/10.1016/j.memsci.2014.05.028

[2] R. Salcedo-Díaz, P. García-Algado, M. García-Rodríguez, J. Fernández-Sempere, and F. Ruiz-Beviá, “Visualization and modeling of the polarization layer in crossflow reverse osmosis in a slit-type channel,” *Journal of Membrane Science,* vol. 456, pp. 21-30, 2014. https://doi.org/10.1016/j.memsci.2014.01.019.

[3] K. Xiao, Y. Shen, and X. Huang, "An analytical model for membrane fouling evolution associated with gel layer growth during constant pressure stirred dead-end filtration," *Journal of Membrane Science,* vol. 427, pp. 139-149, 2013. https://doi.org/10.1016/j.memsci.2012.09.049.

[4] M. Ngo, T. Ueyama, R. Makabe, X. Bui, L. Nghiem, T. Nga, and T. Fujioka, "Fouling behavior and performance of a submerged flat-sheet nanofiltration membrane system for direct treatment of secondary wastewater effluent," *Journal of Water Process Engineering,* vol. 41, p. 10991, 2021. https://doi.org/10.1016/j.jwpe.2021.101991.

[5] A. Vargas, I. Moreno-Andrade, and G. Buitrón, "Controlled backwashing in a membrane sequencing batch reactor used for toxic wastewater treatment,"

Journal of Membrane Science, vol. 320, no. 1-2, pp. 185-190, 2008. https://doi.org/10.1016/j.memsci.2008.03.073.

[6] GB Van den Berg and CA Smolders, "Flux decline in ultrafiltration processes," *Desalination,* vol. 77, pp. 101-133, 1990. https://doi.org/10.1016/0011-9164(90)85023-4.

[7] H. Jiang, Z. Qu, Y. Li, R. Chen, and W. Xing, "One-step semi-continuous cyclohexanone production via hydrogenation of phenol in a submerged ceramic membrane reactor," *Chemical Engineering Journal,* vol. 284, pp. 724-732, 2016. https://doi.org/10.1016/j.cej.2015.09.037.

[8] Z. Trad, C. Vial, J.-P. Fontaine and C. Larroche, "Modeling of hydrodynamics and mixing in a submerged membrane bioreactor," *Chemical Engineering Journal,* vol. 282, pp. 77-90, 2015. https://doi.org/10.1016/j.cej.2015.04.119.

[9] X. Yan, Q. Wu, J. Sun, P. Liang, X. Zhang, K. Xiao, and X. Huang, "Hydrodynamic optimization of membrane bioreactor by horizontal geometry modification using computational fluid dynamics. Bioresource Technology 2016, 200, 328-34.," *Bioresource Technology,* vol. 200, pp. 328-334, 2016. https://doi.org/10.1016/j.biortech.2015.10.050

[10] ZF Cui, S. Chang, and AG Fane, "The use of gas bubbling to enhance membrane processes," *Journal of Membrane Science,* vol. 221, no. 1-2, pp. 1-35, 2003. https://doi.org/10.1016/S0376-7388(03)00246-1.

[11] E. Braak, M. Alliet, S. Schetrite and C. Albasi, "Aeration and hydrodynamics in submerged membrane bioreactors," *Journal of Membrane Science,* vol. 379, no. 1-2, pp. 1-18, 2011.

https://doi.org/10.1016/j.memsci.2011.06.004.

[12] P. Wei, Z. Kaisong, W. Gao, L. Kong, and R. Field, “CFD modeling of hydrodynamic characteristics of slug bubble flow in a flat sheet membrane bioreactor,” *Journal of Membrane Science,* vol. 445, pp. 15-24, 2013. https://doi.org/10.1016/j.memsci.2013.05.036.

[13] X. Liu, Y. Wang, D. Waite, and G. Leslie, “Fluid Structure Interaction analysis of lateral fiber movement in submerged membrane reactors,” *Journal of Membrane Science,* vol. 504, pp. 240-250, 2016. https://doi.org/10.1016/j.memsci.2015.12.056.

[14] M. Mushtaq, M. Bibi, R. Mehmood, M. Amin, K. Sanaullah, and A. Iqbal, “Fluid Dynamics Technique in Membrane Bioreactor Systems,” *Archives of Computational Methods in Engineering,* vol. 31, pp. 641-661, 2024. https://link.springer.com/article/10.1007/s11831-023-09993-y.

[15] K. Feng, C. Li, M. Zhang, and X. Liu, “Simulation and Computational Study of CFD on Tube MBR Membrane Assembly,” *Discrete Dynamics in Nature and Society, Special Issue,* 2021. https://doi.org/10.1155/2021/5577715.

[16] "EVONIK METCell equipment," [Online]. Available: https://www.m-ps.ch/product-and-services/evonik-metcell-equipment

[17] I. Tsibranska, I. Saykova and B. Tylkowski, "Flux and rejection behavior in nanofiltration of polyphenols and flavonoids from," *SCIENTIFIC WORKS OF UNIVERSITY OF FOOF TECHNOLOGIES,* volume L.XII, pp. 514-518, 2015.

https://scholar.google.com/scholar?hl=bg&as_sdt=0%2C5&q=Flux+and+rejection+behavior+in+nanofiltration+of+polyphenols+and+flavonoids+from&btnG=

[18] "ANSYS FLUENT 12.0 Theory Guide," ANSYS Inc. 2009-01-23, [Online]. Available https://www.afs.enea.it/project/neptunius/docs/fluent/html/th/main_pre.htm.

[19] CP Koutsou and A. Karabelas, "Shear stresses and mass transfer at the base of a stirred filtration cell and corresponding conditions in narrow channels with spacers," *Journal of Membrane Science,* vol. 399, pp. 60-72, 2012. https://doi.org/10.1016/j.memsci.2012.01.029.

[20] L. Reiss and T. Hanratty, "An experimental study of the unsteady nature of the viscous sublayer.," *AIChE Journal,* vol.9, no.2, pp. 154-160, 1963. https://doi.org/10.1002/aic.690090204.

[21] L. Peeva, E. Gibbins, S. Luthra, L. White, and R. Stateva, "Effect of concentration polarization and osmotic pressure on flux in organic solvent nanofiltration," *Journal of Membrane Science,* vol. 236, pp. 121-136, 2004. https://doi.org/10.1016/j.memsci.2004.03.004.

[22] [Online]. Available: https://www.ps-prozesstechnik.com/en/membrane-technology/membrane-unit-construction/membrane-filtration-laboratory/membrane-filtration-maximem.html.

Publications and reports of scientific results on the topic of the dissertation

Publications

1. Dzhonova - Atanasova , D., Panjovska , S., Tsibranka , I.. Flow behavior in a stirred dead end filtration cell . Scientific Works of University of Food Technologies, 64, 1, 2017, ISSN:1314-7102, 214-223; https://uft-plovdiv.bg/site_files/file/scienwork/scienworks_2017/docs/3-30.pdf
2. Daniela B. Dzhonova-Atanasova , Iren H. Tsibranska , Stela P. Paniovska . CFD Simulation of Cross-Flow Filtration . Chemical engineering transactions , 70, AIDIC, 2018, ISSN:2283-9216, DOI:10.3303/CET1870341, 2041-2046. SJR:0.293; https://www.aidic.it/cet/18/70/341.pdf
3. I.Tsibranka , D.Dzhonova-Atanasova , St . Panyovska . Effect of variable flux and rejection in membrane separation of polyphenols-containing natural extracts . Journal of Chemical Technology and Metallurgy , 55, 4, University of Chemical Technology and Metallurgy , 2020, ISSN:1314-7471, 765-771. SJR :0.259; https://journal.uctm.edu/node/j2020-4/12_19-170_p_765-771.pdf
4. Tonova , K., Lazarova , M., Dencheva-Zarkova , M., Paniovska , S., Tsibranska , I., Stanoev , V., Dzhonova , D., Genova , J. Separation of glucose , other reducing sugar and phenolics from natural extract by nanofiltration : Effect of pressure and cross-flow velocity . Chemical Engineering Research and Design , 162, October 2020, Elsevier , 2020, ISSN:0263-8762, (Scopus):0.83, JCR-IF (Web of Science):3.35 Q1. https://doi.org/10.1016/j.cherd.2020.07.030

Reports and posters

1. Dzhonova-Atanasova , D., Paniovska , S., Tsibranka , I. Flow Behavior in Dead End Filtration Cell : Experimental Observation and CFD Modelling , Anniversary Tenth Spring Seminar of PhD Students and Young Scientists "Interdisciplinary Chemistry", 21-23.04.2017, Sofia, Bulgaria;
2. S. Panyovska , D. Dzhonova , I Tsibranska , N. Kalassov , R. Manatbaev . CFD modeling of mass transfer through a membrane , optimization of a liquid distributor in a semi-industrial packed column by CFD methods . Sustainable processes , sustainable systems , sustainable environment , 08.11.2019 Sofia, Bulgaria;
3. Nurdaulet Kalassov , Daniela Dzhonova , Irene Tsibranska , Stela Panyovska , Rustem Manatbayev . Application of integrated membrane bioreactors in renewable energy industry optimization of a liquid distributor in a semi-industrial packed column by CFD methods , sustainable processes , Sustainable systems , sustainable environment , 08.11.2019 Sofia, Bulgaria;
4. D. Dzhonova , St. Paniovska , I. Tsibranka , Flow behavior in a stirred dead end filtration cell , International Scientific Conference "Food science , Engineering and Technologies, 2017, 20 - 21.10.2017, Plovdiv , Bulgaria ;
5. D. Dzhonova , P. Velikov , V. Stanev , St. Paniovska , A numerical study of mass transfer in a cross-flow filtration cell , Anniversary scientific conference with international participation "25 years of engineering francophone education at the University of Chemical Technology and Metallurgy", 27-29.09.2017, Sofia, Bulgaria;
6. I. Tsibranska , D. Dzhonova -Atanasova , St. Paniovska , Effect of variable flux and rejection – numerical simulation and experimental evidence in membrane separation of polyphenols-containing natural extracts , Tenth Jubilee

National Conference him/her Chemistry , 26-28.09.2019, Sofia, Bulgaria;

7. Dzhonova-Atanasova , Daniela , Tsibranka , Iren , Paniovska , Stela, CFD simulation of cross-flow filtration , 21st Conference him/her Process Integration for Energy Saving and Pollution Reduction , 25 - 29.08.2018, Prague - Czech Republic;
8. Stela Panyovska , Daniela Dzhonova , Iren Tsibranska , CFD simulation of dead end filtration , 23 Polish Conference on Chemical and Process Engineering , 02 - 05.06.2019, Warsaw, Poland.